ACS OMEGA

http://pubs.acs.org/journal/acsodf

Article

Metronidazole and Ketoprofen-Loaded Mesoporous Magnesium Carbonate for Rapid Treatment of Acute Periodontitis *In Vitro*

Zhaohan Yu, Yan Xiong, Menglin Fan, Jiyao Li,* and Kunneng Liang*

Cite This: *ACS Omega* 2023, 8, 25441−25452

Read Online

ACCESS | Metrics & More | Article Recommendations

ABSTRACT: In the clinical pharmacological treatment of acute periodontitis, local periodontal administration is expected to be preferable to systemic administration. However, the action of the active medicine component is hindered and diminished by the limitation of drug solubility, which does not provide timely relief of the enormous pain being suffered by patients. This study aimed to develop a mesoporous magnesium carbonate (MMC) medicine loading system consisting of MMC, metronidazole (MET), and ketoprofen (KET), which was noted as MET-KET@MMC. A solvent evaporation process was utilized to load MET and KET in MMC. Scanning electron microscopy, nitrogen sorption, thermogravimetric analysis, and X-ray diffraction were performed on the MET-KET@MMC. The rapid drug release properties were also investigated through the drug release curve. The rapid antiseptic property against *Porphyromonas gingivalis* (*P. gingivalis*) and the rapid anti-inflammatory property (within 1 min) were analyzed *in vitro*. The cytotoxicity of MET-KET@MMC was tested in direct contact with human gingival cells and human oral keratinocytes. Crystallizations of MET and KET were completely suppressed in MMC. As compared to crystalline MET and KET, MMC induced higher apparent solubility and rapid drug release, resulting in 8.76 times and 3.43 times higher release percentages of the drugs, respectively. Over 70.11% of MET and 85.97% of KET were released from MMC within 1 min, resisting bacteria and reducing inflammation. MET-KET@MMC nanoparticles enhanced the solubility of drugs and possess rapid antimicrobial and anti-inflammatory properties. The MET-KET@MMC is a promising candidate for the pharmacotherapy of acute periodontitis with drugs, highlighting a significant clinical potential of MMC-based immediate drug release systems.

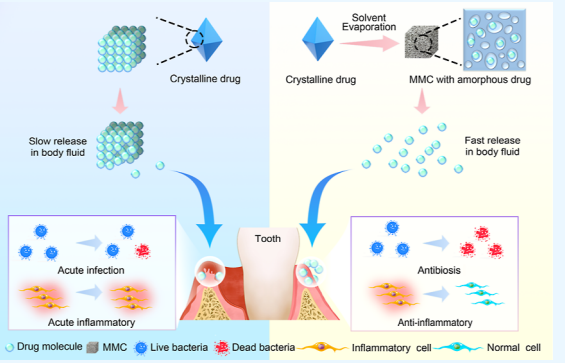

INTRODUCTION

Epidemiologically, periodontitis is among the most worldwide epidemic, afflicting 70% of the adult population older than 65 years in the US.[1] Periodontitis originates from oral pathogens, for instance, *Porphyromonas gingivalis* (*P. gingivalis*), and pathogen-associated inflammation, which cause collateral tissue damage as well as clinical attachment loss.[2] Patients with acute periodontitis, in particular, may experience severe pain, periodontal abscesses, or even systemic complications.[3] One of the main reasons patients seek help from their dentists is to manage periodontal infection or severe pain; hence, appropriate antimicrobial and anti-inflammatory agents were utilized to combat acute infection and sharp inflammation as an adjunct strategy to the surgical approach.[4,5]

Antibiotics and nonsteroidal anti-inflammatory drugs (NSAIDs) are routinely utilized to assist in the medication of periodontal diseases.[6] For instance, metronidazole [MET, 1-(2hydroxyethyl)-2-methyl-5-nitroimidazole] is one of the primary antipathogen agents to treat acute periodontitis.[7] Unfortunately, the antibiotics abuse in the medical domain has posed the risk of leading to antibiotic-resistant bacterial species.[8] In addition, orally administered antibiotics have low concentrations in gingival crevicular fluid and may lead to antibiotic resistance in bacteria.[9] Ibuprofen (IBU) is frequently prescribed as an analgesic in dental treatment due to its efficacy in alleviating mild to moderate pain.[4] Ketoprofen (KET) exhibits superior efficacy compared to IBU in the management of topical pain at therapeutic doses, while also possessing a more favorable benefit−risk profile.[10] Nevertheless, all NSAIDs increase the risk of potentially fatal bleeding and heart attacks or strokes when the drugs are given systemically.[11]

Consequently, local drug delivery has been verified to have the ability to considerably improve medication concentration at the target site while decreasing adverse effects, treatment expense, and drug dosage.[12] In recent years, many under-

Received: April 30, 2023
Accepted: June 13, 2023
Published: July 5, 2023

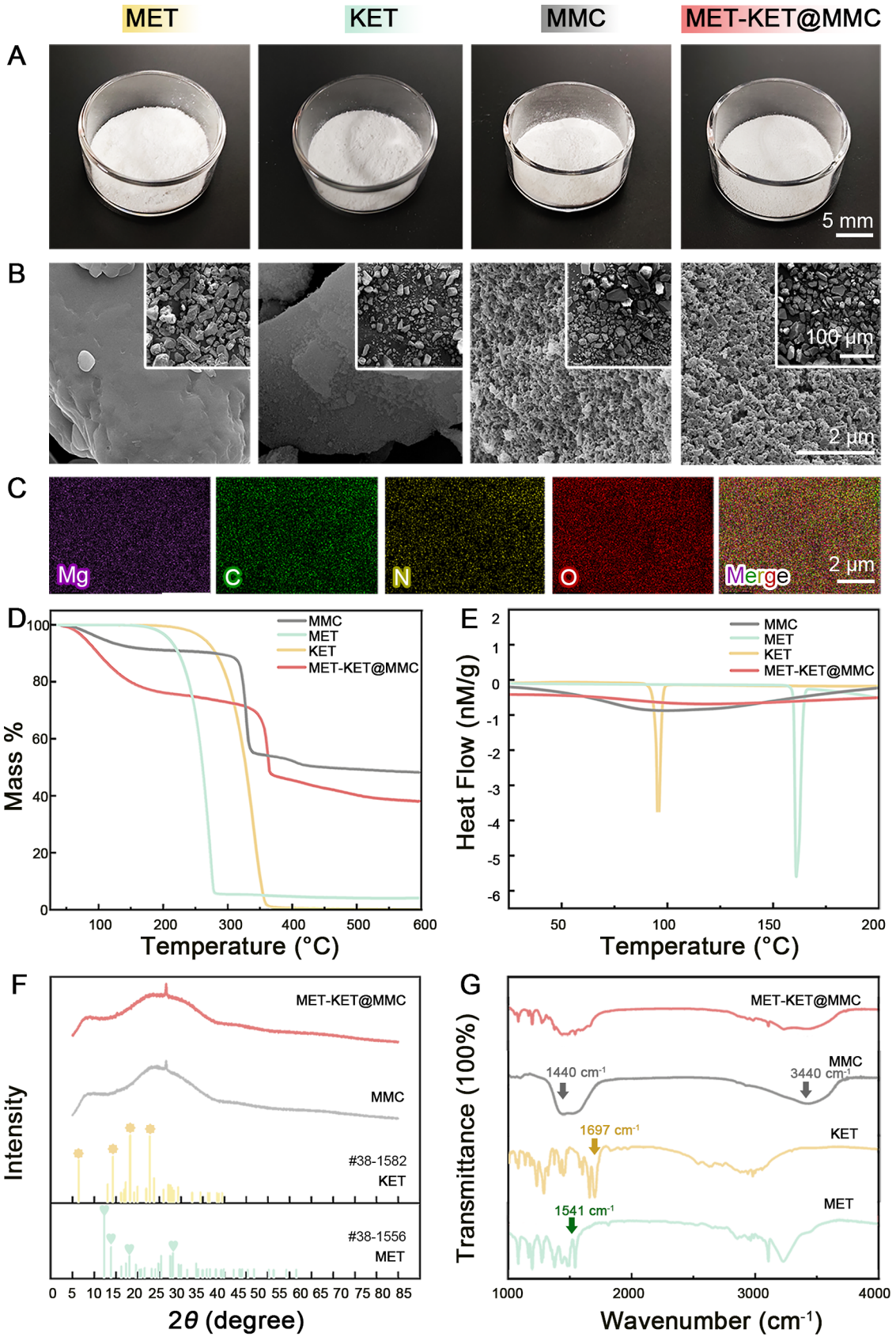

Figure 1. (A) Morphology of MET, KET, MMC, and MET-KET@MMC. (B) SEM images of MET, KET, MMC, and MET-KET@MMC. (C) Elemental mapping of MET-KET@MMC. (D) Normalized mass TGA of MET, KET, MMC, and MET-KET@MMC. (E) DSC curves for MET, KET, MMC, and MET-KET@MMC. (F) XRD patterns for MET, KET, MMC, and MET-KET@MMC. (G) FTIR transmittance spectra for MET, KET, MMC, and MET-KET@MMC.

https://doi.org/10.1021/acsomega.3c02968
ACS Omega 2023, 8, 25441−25452

developed local periodontal materials have been proven to be effective.[13] Low-solubility drugs exhibit delayed attainment of loading dose and inadequate local tissue concentration for the therapeutic efficacy within a short timeframe.[13] Approximately 90% of agents in study and 40% of commercial agents are poorly soluble.[14] The low solubility of these agents is, accordingly, among the primary causes of their low bioavailability.[15] Besides, most recent trials on topical periodontal administration have focused on extended-release materials, which are ineffective for treating acute periodontitis.[16] To date, there is still an unresolved problem with the poor water solubility of topical drugs used for periodontal administration. Additionally, there has been no investigation into the rapid effects of topical periodontal medications.

Various solutions have been proposed to tackle this issue, including formulations of crystalline salts, reductions in active pharmaceutical ingredient (API) particle size, and co−ground combinations.[17] Nevertheless, the effectiveness of formulation techniques is determined by the chemical composition of the agents as well as actual manufacturing issues.[18] For example, the reduction of API particle size may lead to static charge accumulation, resulting in difficulties in handling certain medications.[18] Yao and co-workers loaded 5-fluorouracil into azobenzene-functionalized interfacial cross-linked reverse micelles, relying on the high permeability of small molecules for drug delivery. Although this strategy enhanced the local drug accumulation, it failed to consider the poor solubility of the insoluble drug itself.[19] However, recent studies have revealed that the crystallization of drugs could be restrained when they are embarked into mesoporous holes with pore diameters, ranging from 2 to 50 nm.[20] Mesoporous magnesium carbonate (MMC) has recently been synthesized, exhibiting a narrow distribution of pore sizes and a wide superficial area.[21,22] The amorphous forms of several poorly water-soluble compounds have been stabilized by loading them into MMC, resulting in increased solubilities and faster dissolution rates.[23−25] This implies that MMC could fundamentally alter the solubility characteristics of the drug, converting crystalline low water-soluble medications into amorphous water-soluble medications.[26] MMC improves solubility by increasing the amount of insoluble drug dissolved. Drug solubilization enables a rapid increase in the local drug concentration in a short period of time, resulting in rapid release.[26,27] Therefore, the utilization of MMC is anticipated to serve as a highly efficacious strategy in enhancing the bioavailability of poorly water-soluble medications for treating acute periodontitis.[28] Nonetheless, there have been no studies on MMC as a topical treatment for acute periodontitis.

Herein, a MET-KET@MMC drug immediate-release system was established through a simple solvent evaporation method, using the commonly used oral antibiotic MET and KET. The MET and KET in MMC were rapidly released to achieve effective drug concentrations within 1 min, providing antibacterial and anti-inflammatory effects. Our work has led to the first use of the immediate-release carrier MMC in the field of pharmacological treatment of acute periodontitis.

RESULTS AND DISCUSSION

In this study, MET and KET were loaded into MMC simultaneously for the first time. Both MET and KET have small molecular weights and could therefore access the pores of MMC.[22,23,25] After dissolving in ethanol, the drug molecules free in solution were adsorbed into the pores of the MMC surface.[22] As shown in Figure 1A, MET, KET, and MET-KET@MMC were white powder. Scanning electron microscopy (SEM) of MET, KET, MMC, and MET-KET@MMC is shown in Figure 1B. The surface of MMC had a concave and convex porous morphology. No major morphological changes were noted after loading drugs. Figure 1C illustrates the distribution of Mg, C, N, and O elements, thus indicating the incorporation of MET and KET. The results of thermogravimetric analysis (TGA) are shown in Figure 1D. The decomposition of the unloaded MMC took place at approximately 380 °C. At lower temperatures, crystallographic MET and KET decomposed almost completely (280 °C for MET and 350 °C for KET). The TGA curves of MET-KET@MMC indicate that no discernible mass loss occurred at the temperatures where crystalline MET and KET would typically decompose. The TGA profiles revealed a significant disparity in weight loss between MMC and MET-KET@MMC, which corresponded to the loading of both MET and KET (Figure 1D). Since MMC tends to absorb water, the quality decreased as the water in MMC and MET-KET@MMC evaporated in the range of 100−200 °C. Notably, the decomposition temperature of drug-loaded MMC was higher than that of unloaded MMC. The temperature elevation in this process can be accounted for by the Kelvin equation, which states that within the pores of MMC, the boiling point of the liquid will increase due to a rise in vapor pressure.[23,29] This appearance has previously been noticed in the mesoporous drug carrier.[23,29] In the differential scanning calorimetry (DSC) pattern, the absence of peaks corresponding to MET (at 160 °C) and KET (at 95 °C) indicates that drugs were incorporated in an amorphous state (Figure 1E). Previous attempts to incorporate additional APIs into the MMC resulted in drug crystallization within the pores of carrier materials.[23] In contrast, the X-ray diffraction (XRD) of this experiment indicates that neither 10% wt of MET nor KET showed crystallization, demonstrating that there was no crystallization outside the pores of MMC (Figure 1F). The lack of the peaks of crystalline drugs indicated that the MET and KET incorporated into MMC were amorphous.[25] Without MMC, the drug molecules in solution precipitated as crystals when the solvent evaporated. In contrast, after the drug molecules were absorbed into the pores of MMC, the mesoporous structure had an area-bound effect when the solvent was evaporated. This effect stopped the nucleation and crystal growth of identical molecules, which kept the drug in an amorphous form.[30] The absence of crystalline drug peaks suggests that the MET and KET incorporated into MMC were amorphous.[25] In the Fourier transform infrared spectroscopy (FTIR) spectra (Figure 1G), the absorbance band at ∼3440 cm^{-1} corresponded to adsorbed water. Bands at ∼1400 cm^{-1} correspond to the carbonate group. The overlapping absorption bands from MET and KET (1541 and 1697 cm^{-1}) in MET-KET@MMC indicated that MET and KET were loaded into MMC.[31] The FTIR spectra of MET-KET@MMC samples did not exhibit any new absorption bands, except for those observed in the absorption spectra of free KET and MET samples, indicating that the adsorption of MET and KET onto the pore walls was physical rather than chemical.[23] The Brunauer−Emmett−Teller (BET) surface areas and pore volumes are presented in Table 1. The surface area and pore volume were reduced after drugs were loaded. This supports the results of XRD and DSC, indicating that MET and KET had actually entered the mesoporous structure

https://doi.org/10.1021/acsomega.3c02968
ACS Omega 2023, 8, 25441−25452

Table 1. SSA and Pore Volume of Unloaded and MET-KET@MMC

	MMC	MET-KET@MMC
SSA	226.4022 m^2/g	103.2685 m^2/g
pore volume	0.83 cm^3/g	0.21 cm^3/g

of MMC. From the foregoing, we could consider that MET and KET were successfully loaded into MMC. The crystallizations of MET and KET were completely suppressed by the mesoporous structure of MMC.[32]

Dissolution is the rate-limiting process of absorption and consequently the limiting step of bioavailability.[33] The rapid dissolution of the drug allows for its absorption in the body at the fastest possible rate, thus allowing the drug to react in a short time, which is significant for the relief of the sufferings of patients. Albeit short-term, quick release offers the benefit of the immediate therapeutic effect.[34] It is imperative to investigate the capacity of MMC for prompt co-delivery of both drugs. Figure 2A illustrates the dissolution curves of crystallography. Figure 2A shows the dissolution profiles of MET, KET, and MET-KET@MMC in phosphate buffer saline (PBS). According to the concentration released from MET-KET@MMC, the entrapment efficiency and drug loading of MET and KET were 88.33% ± 0.99 and 7.36% ± 0.08, and 94.82% ± 1.23 and 7.90% ± 0.10, respectively (Table 2).

Table 2. Entrapment and Drug-Loading Efficiencies

	entrapment rate	drug-loading rate
MET	88.33% ± 0.99	7.36% ± 0.08
KET	94.82% ± 1.23	7.90% ± 0.10

Evidently, the dissolution kinetics of amorphous MET and KET in MMC were superior to those of their crystalline counterparts. During the initial minute, the release of MET from MMC was 8.76-fold higher than that from crystalline MET; similarly, the release of KET from MMC was 3.43-fold higher than that from crystalline KET (Figure 2A). Apparently, within the MMC, the dissolution efficiencies of amorphous

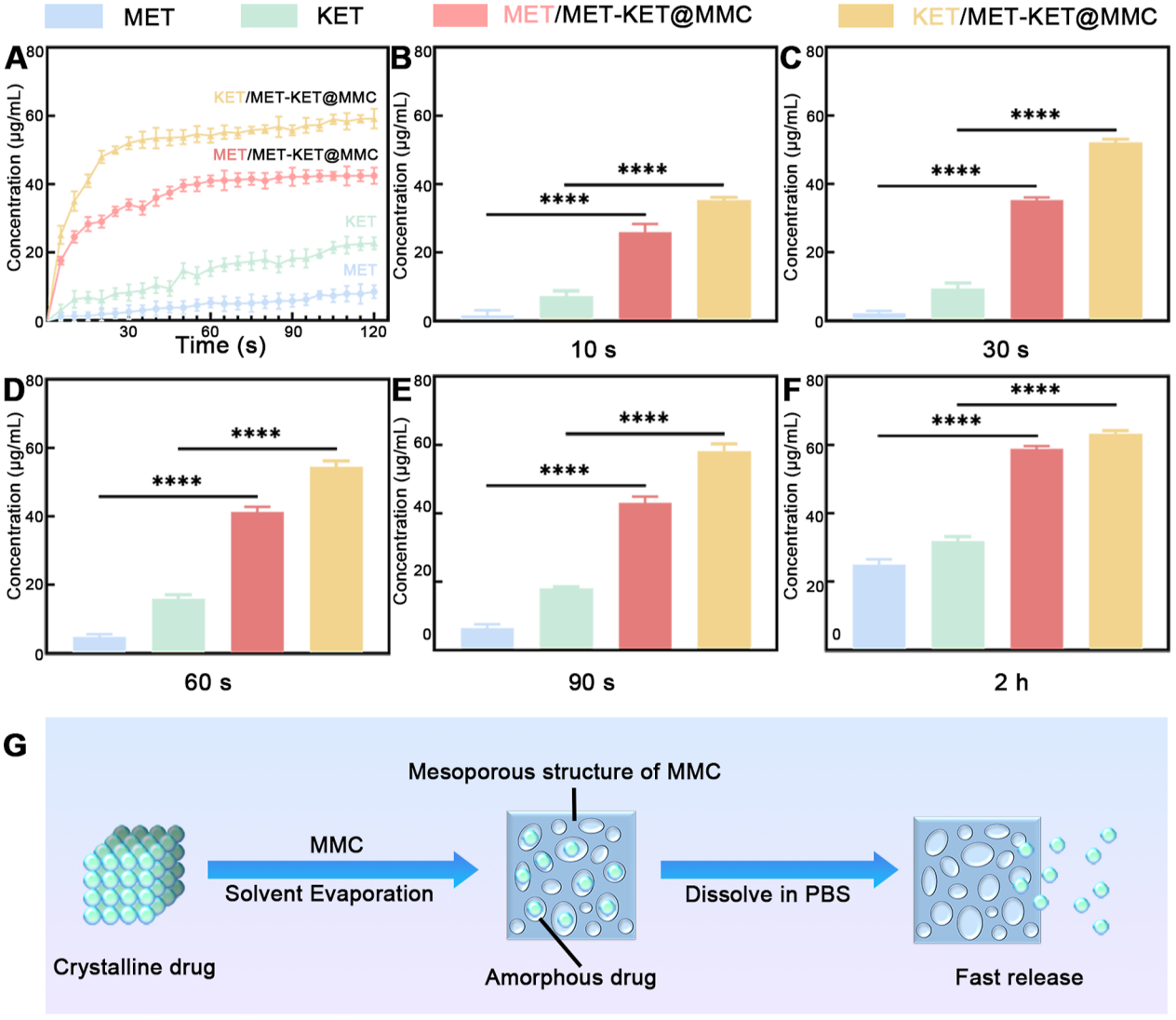

Figure 2. Drug release properties. (A–F) Dissolution profiles for MET, KET, and MET-KET@MMC in PBS. (G) Possible mechanism of the solubilization of MMC for insoluble crystalline drugs. The crystalline drug was dissolved in alcohol, allowing the drug molecules to infiltrate into the mesoporous structure of the MMC. The mesoporous structure maintained the drug molecules in the non-crystalline state. Mean ± SD is shown (n = 3). **** represents $P < 0.0001$.

https://doi.org/10.1021/acsomega.3c02968
ACS Omega 2023, 8, 25441−25452

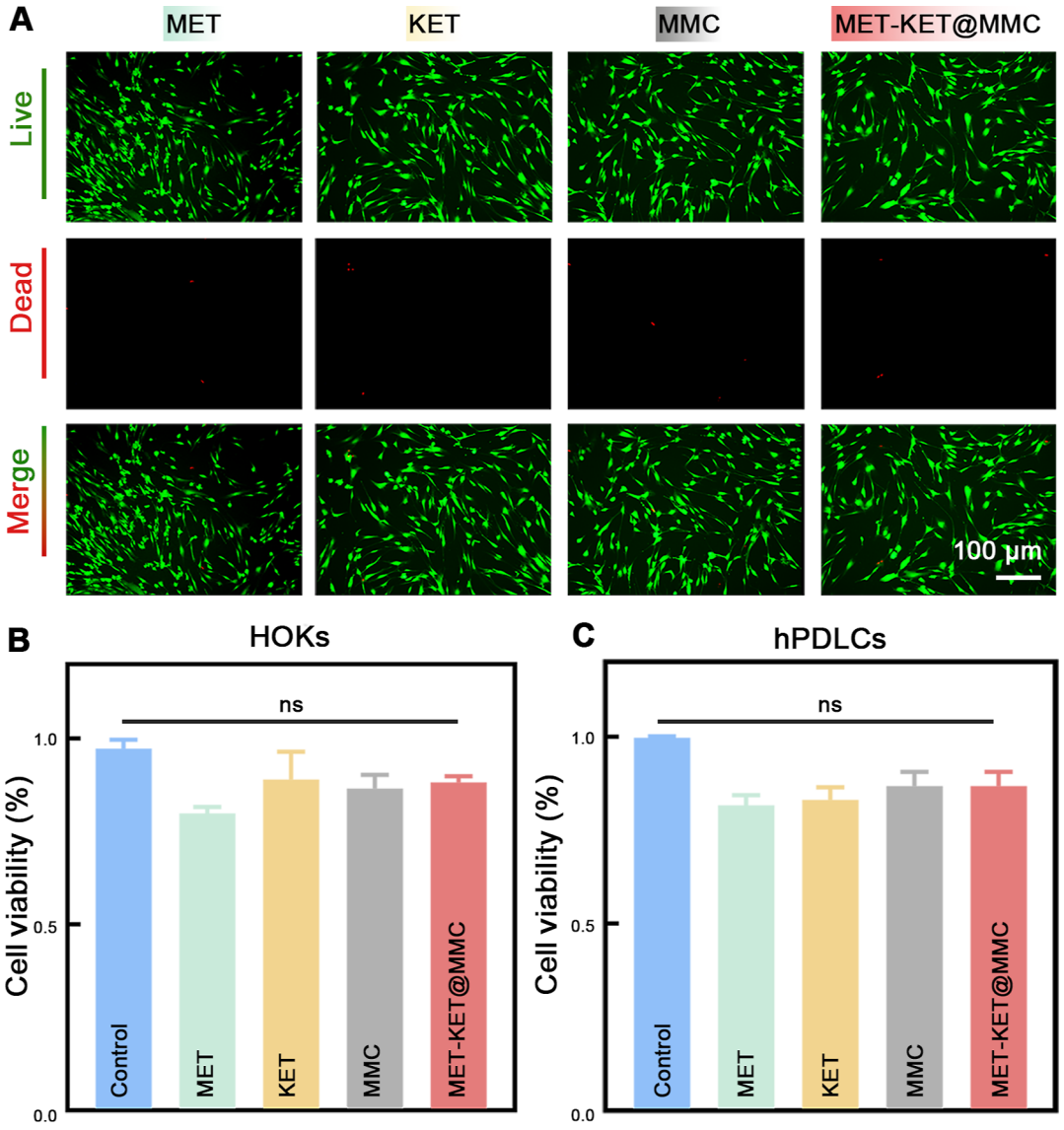

Figure 3. Cell viability of hPDLCs cultured in studied samples after 24 h and compared to growth media only. (A) Live/dead staining of hPDLCs. (B,C) CCK-8 assay of hPDLCs and HOKs. Viability of samples containing MMC presented acceptable cytotoxicity compared with the control group (1000 μg/mL) (mean ± SD, $n = 6$) ($P < 0.05$). n.s. indicates no significant difference.

MET and KET were higher than those of the free crystalline substances. Over 70.11% of MET and 85.97% of KET were released from MMC within 1 min (Figure 2B–E). After 2 h, the final concentrations of MET and KET released from MMC were 8.37 and 9.46 μg/mL. For a comprehensive assessment of the impact of the carrier on drug release, we recorded and presented 5 time points of the drug concentration (as shown in Figure 2B–E). The concentrations of MET and KET released from MMC were significantly higher than those of crystalline MET and KET in all 5 time points ($P < 0.0001$). The observed rapid release and dissolution of the drugs within the carrier pore structure do not affect the ultimate dissolved drug levels. The final concentrations of MET and KET were 8.37 and 9.46 μg/mL, while the final concentrations of MET and KET in MMC were elevated to 58.21 and 42.37 μg/mL, respectively. It can be observed that both drugs were released rapidly from MMC. The input amounts in PBS of crystalline MET and KET were basically the same as the actual drug loading in MMC, while more drugs were released in MMC during the same time. Crystalline drugs were dissolved in alcohol and turned into a free state (Figure 2G). The drug molecules were subsequently adsorbed into the mesoporous structure of the MMC. The crystalline propagation was blocked by the confinement of the mesoporous structure; hence, the drugs were stabilized in their amorphous forms, which is attributed to the interactions between APIs and pore walls, alterations in nucleation mechanisms, and kinetics within mesopores.[23,32,35] The mechanisms for the increased solubility are as follows: (1) when the amorphous molecules in MMC were in contact with water molecules, they could diffuse directly into the aqueous solution because there was no process to overcome the intermolecular forces from the crystal structure.[21] Thus, the insolvable drugs in MMC could be rapidly dissolved in water (Figure 2G); (2) according to the Noyes–Whitney equation, the rate of dissolution is directly proportional to the surface of particles and the solubility of their respective solvents. Therefore, it is a viable approach to enhance drug solubility through the expansion of surface area. In the present study, MET and KET were absorbed in the surface pores of MMC in their non-crystalline states, which expanded the contact area

https://doi.org/10.1021/acsomega.3c02968
ACS Omega 2023, 8, 25441–25452

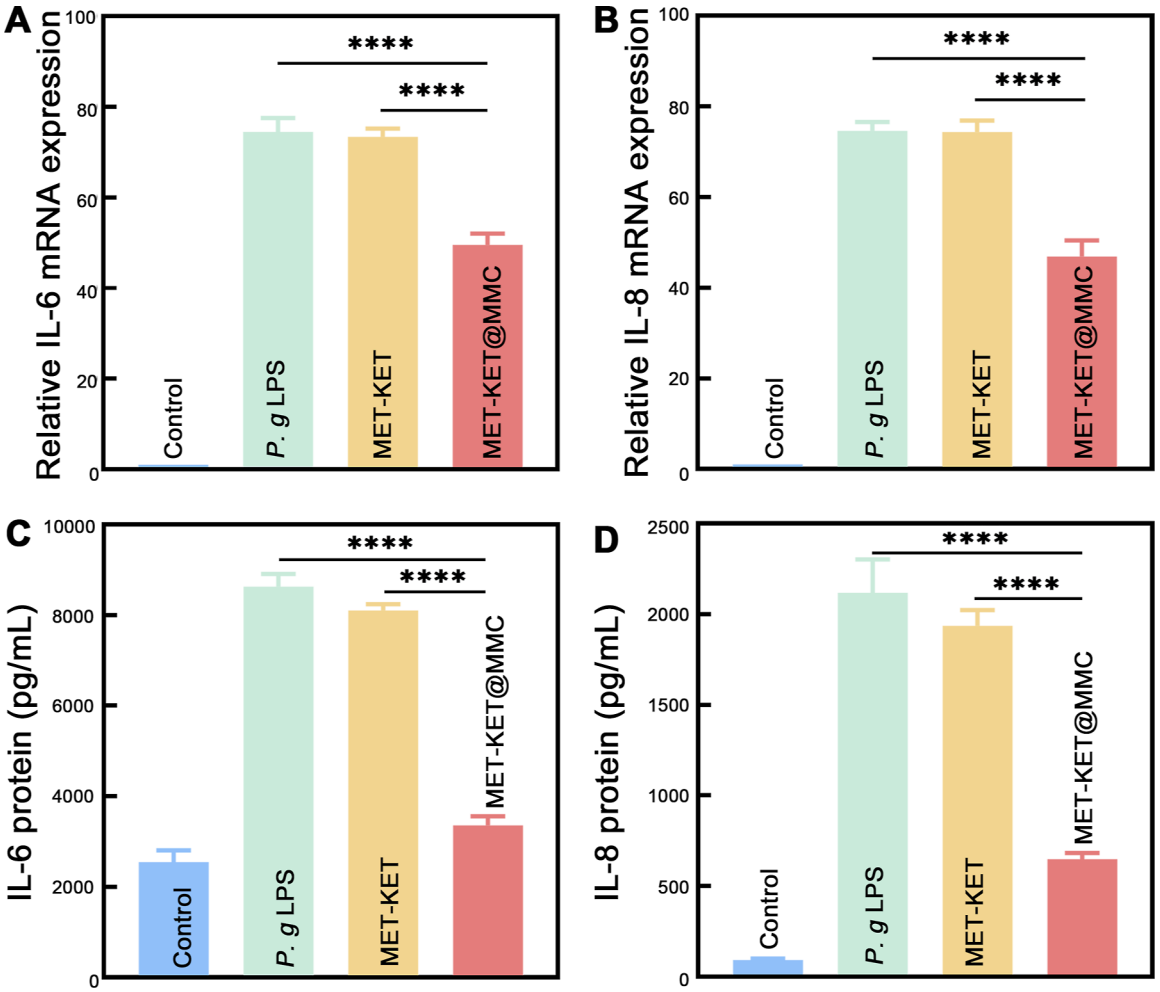

Figure 4. Anti-inflammatory effects of MET-KET and MET-KET@MMC on (A,B) cytokine and (C,D) protein expression of IL-6 and IL-8 in hPDLCs and HOKs stimulated with 10μg/mL *P. g* LPS. Mean ± SD is shown (mean ± SD, $n = 3$). The drug released from MET-KET@MMC in 1 min has been able to take an anti-inflammatory effect. **** represents $P < 0.0001$.

with water. The solubilities of MET and KET were boosted, and the drug concentrations elevated rapidly within a short time.

Although MMC has been considered safe, we evaluated the cytotoxicity of MET-KET@MMC. As shown in Figure 3A, the live/dead staining of human gingival cells (hPDLCs) confirmed a non-toxic effect of MET-KET@MMC. The live cells of MET-KET@MMC were morphologically comparable to other groups. Figure 3B,C demonstrates that the viability of hPDLCs and human oral keratinocytes (HOKs) exposed to MET-KET@MMC (1 mg/mL) did not exhibit a significant decrease in comparison to the control cells ($P < 0.0001$). MMC has been classified as "Generally Recognized as Safe" (GRAS) by the FDA. One study reported that MMC preparations administered orally to male rats did not show toxicity to rats.[20] Furthermore, in this study, the clinical application scenario for MMC was a periodontal rinse. Residual MMC was readily removed by the mouthwash, and there was little physical harm from the low cytotoxicity of MMC.

In the pathology of periodontitis, periodontal pathogens and cellular immune responses are two major factors.[36] *P. g* LPS has been used to induce immune responses in a number of studies around periodontal diseases.[13,37] hPDLCs in periodontal ligaments recognize pathogenic factors and play a significant role in the innate immune response.[38] Hence, *P. g* LPS was utilized to simulate the inflammatory state of hPDLCs infected with *P. gingivalis* in this study.[39] Connective tissue injury and alveolar bone loss are induced by the pro-inflammatory cytokines IL-6 and IL-8.[40] Therefore, we assessed the level of cellular inflammation by evaluating IL-6 and IL-8. The translational level and protein quantification, which were separately measured by real-time polymerase chain reaction (PCR) and enzyme-linked immunosorbent assay (ELISA) after 24 h of culturing with *P. g* LPS, are shown in Figure 4. After being stimulated by *P. g* LPS, IL-6 levels increased (~3-fold at the transcriptional level and ~3.24-fold regarding protein production) compared to control cells (Figure 4A,C). Relative to the MET-KET group, the expression levels of IL-6 and IL-8 were reduced in the MET-KET@MMC group (Figure 4B,D). The expression of IL-6 and IL-8 was considerably lower in the MET-KET@MMC group compared to the MET-KET group because of the higher KET concentration ($P < 0.0001$). This indicated that the anti-inflammatory agents released from MET-KET@MMC in only 1 min suppressed LPS-mediated cytokine production in hPDLCs. There was no statistically significant difference observed between the groups treated with *P. g* LPS and MET-KET. These results indicated that the inflammatory gene expression and the protein level could be significantly reduced

https://doi.org/10.1021/acsomega.3c02968
ACS Omega 2023, 8, 25441−25452

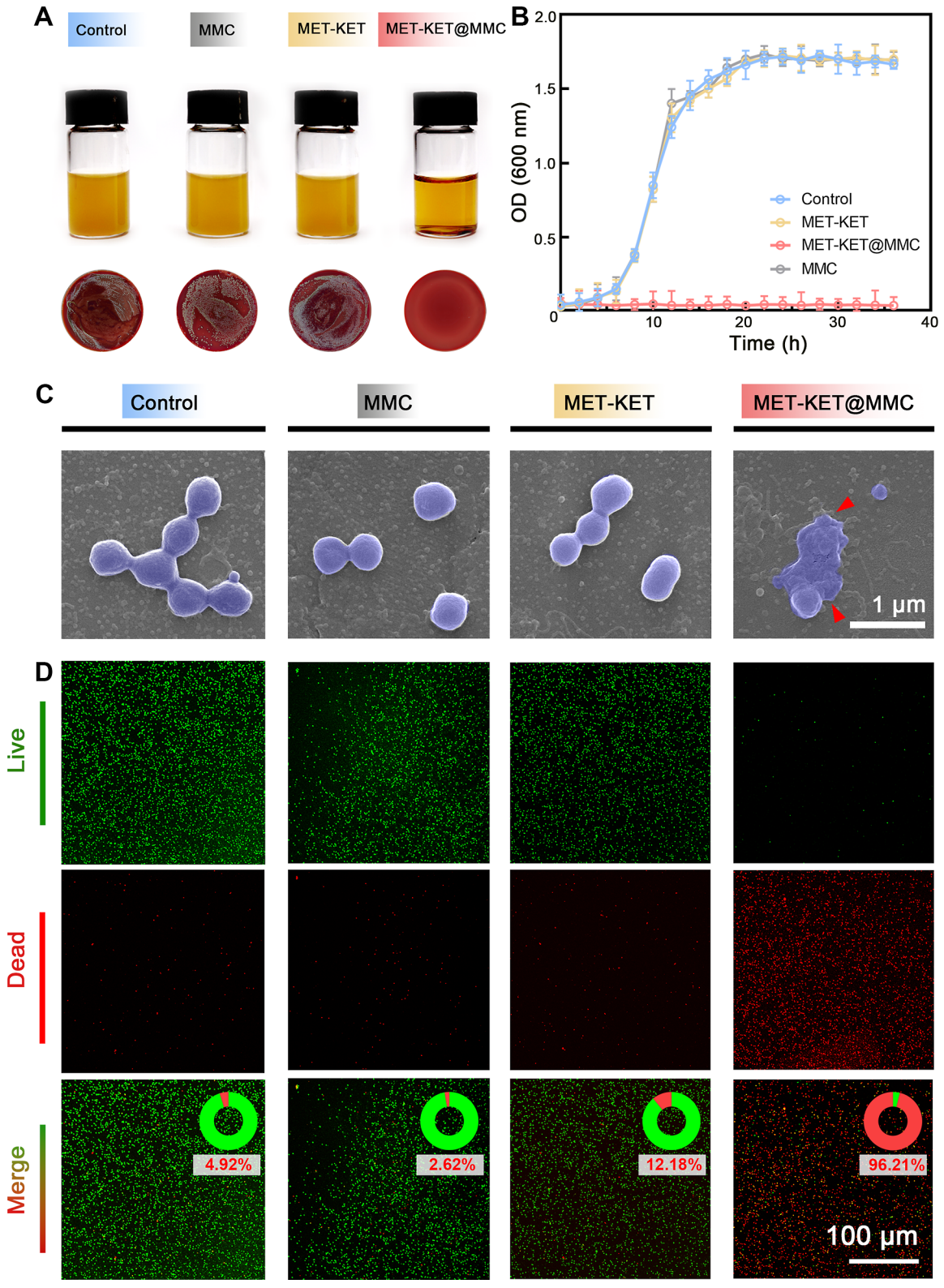

Figure 5. Rapid antibacterial ability of MET-KET@MMC within 1 min. (A) BHI and agar plates of each group. The BHI of the MET-KET@MMC group is clarified, and there is no colony present on the agar plate. (B) Growth curves of MMC, MET-KET, MET-KET@MMC, and the control group without antibacterial agent. The antibiotic released from MET-KET@MMC in 1 min prevented the growth of *P. gingivalis*. (C) SEM micrographs of titanium discs incubated with studied samples after 2 d. The *P. gingivalis* were in normal shape in the MMC group and MET-KET group compared with the control group, while damaged bacteria could be observed on the titanium discs in the MET-KET@MMC group. (D) Live/dead staining images. The green fluorescence represented the live germs, while the red one denoted the dead. The MET-KET@MMC group shows the strongest red fluorescent signal.

https://doi.org/10.1021/acsomega.3c02968
ACS Omega 2023, 8, 25441−25452

by KET, which was rapidly released from MMC in 1 min, while the drug released from crystalline MET-KET in 1 min had no significant anti-inflammatory effect ($P < 0.0001$).

The spread plate method proved that the antibiotic loaded in MMC was sufficient to kill *P. gingivalis*. The antibiotic constituents released from crystalline MET within 1 min exhibited a negligible killing effect against *P. gingivalis* (Figure 5A). The time−kill curves demonstrated the rapid efficacy of MET-KET@MMC against periodontal pathogens, demonstrating that the antibiotic agents released from MET-KET@MMC in just 1 min are sufficient to eradicate pathogens (Figure 5B). In contrast, a drastic decrement in microbe colonies appeared in the MET-KET@MMC group, where almost 100% of *P. gingivalis* were killed (Table 3). Damaged bacteria were observed on the titanium disc incubated with MET-KET@MMC, while no remarkable difference in bacterial form was found between the titanium disc incubated with MMC, MET-KET, and the control titanium disc (Figure 5C). The immediate killing effects were verified by live/dead staining (Figure 5D). *P. gingivalis* in the control group, MMC group, and the MET group displayed obvious green fluorescence. In contrast, 96.21% of dead bacteria (red fluorescence) was observed in the MET-KET@MMC group, indicating that MET released within 1 m resulted in rapid bacterial killing. These consequences were due to the rapid release of MET from MMC. In this study, a high concentration of MET was released from MMC in a short time, while crystalline MET only possessed a little antimicrobial property on account of its poor solubility. The rapid antibiotics process corresponds to the clinical treatment principle of using a large dose of antibiotics as the infection appears.[22] Additionally, a previous study has demonstrated that MMC possesses antimicrobial properties attributed to the generation of reactive oxygen species, direct contact with microorganisms, and its alkaline effect.[40] From these results, the drug released from MMC in 1 min showed antibiotic bacteriostasis against *P. gingivalis*, while the APIs released from crystalline drugs had no antibacterial effect due to the lower medicine concentration, according to the release curve and antiseptic test results. Given the above, MMC nanoparticles possess a wide field of application prospects in the treatment of acute periodontitis as well as various acute microbial infections.

Table 3. Antibacterial Efficiencies

	antibacterial rate[a]
control	1.48% ± 0.01[a]
MMC	3.14% ± 0.01[a]
MET-KET	5.35% ± 0.02[a]
MET-KET@MMC	100% ± 0.00[b]

[a]Dissimilar letters (a and b) indicate significantly different values (mean ± SD, $n = 3$, $P < 0.05$).

Our study demonstrated that MMC released both drugs rapidly and enabled drug concentrations to reach effective antibacterial and anti-inflammatory levels within brief periods. MET-KET@MMC could be applied in injectable pastes or flushes to rinse swollen gums and periodontal pockets in patients with acute periodontitis. The rapid release of MET and KET from MMC would provide a rapid bactericidal and anti-inflammatory effect, thus relieving the pain of patients and eliminating swelling. Furthermore, MMC is not specific for loading drugs and can be loaded with various insoluble small molecules such as IBU, tolfenamic acid, and rimonabant.[23,25] It is conceivable that the use of MMC loaded with insoluble broad-spectrum antibiotics would be beneficial in the treatment of various acute infections. Therefore, MMC is anticipated to be used as a direct topical delivery agent for the treatment of skin infections and bone infections. In view of the intricate and diversified microenvironment of periodontal microbial communities, the effects of MMC as a fast-release carrier on multi-microbial or clinically relevant animal models are worth further proving. In summary, MMC, as an efficient fast-release drug carrier, could load diverse insoluble agents. If further developed, this technology is expected to be applied to a variety of acute dental infections for rapid relief of patient suffering.

CONCLUSIONS

In this study, we innovatively prepared a dual-functional topical rapid-release drug formulation, MET-KET@MMC, with antibacterial and anti-inflammatory functions, which was expected for the treatment of acute periodontitis. MET-KET@MMC possessed a faster release and dissolution compared to the dissolution of crystalline MET and KET. The rapid killing efficacy against periodontitis-related pathogens and rapid anti-inflammatory properties have also been confirmed *in vitro*, which would be beneficial to patients suffering from acute periodontitis. MET-KET@MMC did not show cell toxicity toward hPDLCs and HOKs. This work paves the way for further investigations of MMC as a pharmaceutical carrier in topical formulations targeting different types of acute oral infections and inflammation.

MATERIALS AND METHODS

Synthesis of MMC. MMC was prepared by a combination of solvothermal synthesis, as described previously.[25] In brief, 3 g of MgO (Sigma-Aldrich Inc., St. Louis, MO, USA) was put into 45 mL of CH_3OH (Sigma-Aldrich Inc., St. Louis, MO, USA) with stirring at 500 rpm under 4 bar CO_2 for 4 d at room temperature. Subsequently, air pressure was released, and the 5 mL of suspension in the reaction was slowly dropped to 250 mL of ethyl acetate at 25 °C. The resulting suspension was then continuously stirred until all of the solvents had evaporated in a well-ventilated area, leaving only a dried powder. To remove any residual organic groups formed during the reaction, the powder was heated to 250 °C for 30 min at a temperature ramp rate of 1 °C/min. The MMC was stored in a dry environment.[25]

Drug-Loading Procedure. MET and KET (Sigma-Aldrich Inc., St. Louis, MO, USA) were incorporated into MMC *via* a simple solvent evaporation method to obtain MET-KET@MMC. Specifically, 25 g of MET and 25 g of KET were dissolved in 500 mL of ethanol, followed by the addition of 200 g of MMC into the solution. The mixture was subjected to orbital shaking at 500 rpm for 2 day at a temperature of 25 °C to facilitate drug diffusion into the porous structure of MMC. Subsequently, the solution was subjected to heating at 80 °C in an oven for alcohol evaporation and blended to achieve homogeneity.[25]

Characterization of MET-KET@MMC. *SEM and Energy-Dispersive Spectroscopy.* MET, KET, and MET-KET@MMC were examined *via* SEM equipped with energy-dispersive spectroscopy mapping (Inspect F50, FEI, USA). Images were

https://doi.org/10.1021/acsomega.3c02968
ACS Omega 2023, 8, 25441−25452

recorded with an acceleration voltage of 3 kV using the in-lens detector.[41]

Differential Scanning Calorimetry. DSC was performed with a DSC instrument (Netzsch, GER). Specimens of 3.5−5.5 mg were frozen at −20 °C and subsequently heated to 270 °C (3 °C min^{-1}) under a N_2 atmosphere. The temperature elevation process was accompanied by the recording of heat flow.

Thermal Gravimetric Analysis. The mass of 15 mg of samples was recorded as they were heated from 30 to 600 °C at a rate of 3 °C/min under a nitrogen atmosphere using a TGA instrument (Mettler Toledo TGA/SDTA851e).

X-Ray Diffraction. XRD was performed after MMC and MET-KET@MMC had been placed on a silicon holder (Ultima IV, Rigaku, Japan). The patterns were collected in the 2θ range from 5° to 80° at a rate of 0.02 °/s. Standard cards for MET and KET were obtained from Jade software.

Fourier Transform Infrared Spectroscopy. Samples were ground with potassium bromide and pressed to slices.[42] FTIR analyses were carried out using Fourier transform infrared spectroscopy (NICOLET is 50, Thermo Scientific, USA) from 350 to 4400 cm^{-1} at 25 °C.[43]

Nitrogen Sorption Analysis. At first, samples got degassed under vacuum for 12 h at 90 °C. The SSA was determined using the BET method. The total pore capacity was determined through single-point adsorption ($P/P_0 \approx 1$). The ASAP 2020 (Micromeritics) was employed for all computations.[44]

In Vitro Drug Release Measurement. 10 mg of MET and 10 mg of KET were dissolved in a vessel containing 1500 mL of PBS at 37 °C with a stirring rate of 100 rpm. 100 mg of MET-KET@MMC was dissolved in another vessel containing 1500 mL of PBS under the same condition.[25] As the same volume of fresh PBS was blended into the medium at the same moment, 0.5 mL aliquots were collected from each vessel and filtrated *via* a 0.2 m nylon filter (Servicebio, China).[25] The liquid samples were measured by a Nanodrop 2000 spectrometer (ThermoScientific, Waltham, MA, USA). Absorbance measurements were conducted at 320 nm (MET) and 255 nm (KET).[42] The concentrations of MET and KET were obtained *via* standard curves corresponding to the known dissolved MET and KET values. The measurements were carried out three times, and the standard and mean concentration values were also computed. The entrapment efficiency and drug loading of MET and KET were determined by the following calculations

$$\text{entrapment efficiency (\%w/w)} = \frac{\text{weight of drug in MMC}}{\text{theoretical weight of drug in MMC}} \times 100$$

$$\text{drug loading efficiency (\%w/w)} = \frac{\text{weight of drug in MMC}}{\text{weight of MMC}} \times 100$$

Cell Culture. hPDLCs were obtained from healthy human premolar periodontal ligaments. Following extraction, the premolars were rinsed five times using PBS. Peripheral tissues of the middle third surface of tooth roots were scraped off and digested using collagenase type I (1 mg/mL, HyClone, UT, USA) at 37 °C for 0.5 h. The tissues were cultured in α-MEM medium (Gibco, Grand Island, NY, USA) with 10% fetal calf serum (Gibco, Grand Island, NY, USA), penicillin (100 U/mL, Servicebio, China), and streptomycin (100 g/mL, Servicebio, China). hPDLCs were passaged by trypsin after the cells had adhered and spread across the plate wall, and the cultures used for our experiments were those between passages 3 and 7.[45,46] Besides, HOKs were grown for 24 h.

In Vitro Cytotoxicity/Viability Assay. Cell viability was accessed using a cell counting kit-8 (CCK-8, Servicebio, China) assay.[47] Cytotoxicity was evaluated in hPDLCs. hPDLCs and HOKs were incubated for 1 d and then inoculated in treated 96-well plates with medium containing MET, KET, MMC, and MET-KET@MMC (1 mg/mL) for 24 h, respectively. The seeding density was 5000 cells/well in 100 μL. According to the directions, cell viability was measured every 2 d. The absorbance was measured at 450 nm against a medium-only baseline.

The following formula was used to calculate cell viability

$$\frac{\text{OD of sample} - \text{OD of baseline}}{\text{OD of control} - \text{OD of baseline}} \times 100$$

Evaluation of Anti-inflammation Activities. In order to verify the solubilization capacity of MMC, all the samples were dropped in solution (α-MEM medium) for 1 min under the same conditions, and only the solution was collected after being filtrated through a 0.2 mm cylinder filter for the follow-up experiments. To be consistent with the practical drug concentration of MET-KET@MMC, MET and KET (MET-KET) were added to solutions in the same mass. As previously described, ultrapure lipopolysaccharide from *P. gingivalis* (*P. g* LPS) (Invivogen, San Diego, USA) *in vitro*, *P. gingivalis* was employed to emulate conditions of inflammation: 1×10^6 hPDLCs per well were cultivated in a 25 mm^2 culture dish. After 24 h serum starvation, hPDLCs were irritated with *P. g* LPS (10 μg/mL) for 1 d.[45] Then, the hPDLCs were rinsed with normal saline and incubated separately in the culture medium mentioned above. The hPDLCs that were incubated with pure α-MEM medium subsequently were referred *t* as a negative control group.

Enzyme-Linked Immunosorbent Assay. Human IL-6 and IL-8 ELISA kits (Jiangsu Meimian Industrial Co., Ltd) were employed to measure the levels of interleukin-6 (IL-6) and interleukin-8 (IL-8) in the culture supernatants according to the manufacturer's instructions.[45]

Quantitative Reverse Transcription PCR (RT-qPCR). After a 24 h incubation, TRIzol reagent (Invitrogen) was used to extract mRNA according to the instructions.[45,46] The RNA was reverse-transcribed into cDNA using the Rayscript cDNA Synthesis KIT (GENEray, GK8030, Shanghai, China) and subsequently employed in RT-PCR reactions with SYBR Green (GENEray, GK8030, Shanghai, China). Table 4 describes the primers of cytokines. Reactions were carried out on an ABI7500 apparatus (Applied Biosystems Inc., USA).

Table 4. Primers of Cytokines

cytokines	primer sequence
IL-6 F	F: TGCAATAACCACCCCTGACC
IL-6 R	R: GTGCCCATGCTACATTTGCC
IL-8 F	F: TTTTGCCAAGGAGTGCTAAAGA
IL-8 R	R: AACCCTCTGCACCCAGTTTTC
GADPH F	F: CCAGAACATCATCCCTGCCT
GADPH R	R: CCTGCTTCACCACCTTCTTG

https://doi.org/10.1021/acsomega.3c02968
ACS Omega 2023, 8, 25441−25452

Before being compared with the control, the level of mRNA to be tested was standardized to the level of GAPDH. Relative game expression levels were quantitated using the ΔΔCt method.[48]

Evaluation of Antibacterial Activity. Bacteria Culture. *P. gingivalis* (ATCC33277, China) was cultivated in brain−heart infusion broth medium (BHI, Difco, Sparks, MA, USA) with hemin (5 mg/mL) and vitamin K1 (1 mg/mL) at 37 °C under anaerobic conditions (80% N_2, 10% H_2, and 10% CO_2) in 96-well plates for 2 d. The amount of *P. gingivalis* was estimated by the absorbance of cultured germs at 600 nm utilizing a microplate reader (Multiskan Go, Thermo Scientific), corresponding to 1×10^8 bacteria/mL. The *P. gingivalis* was diluted to 3×10^7 colony-forming units (CFUs)/mL before use.[22]

Spread Plate Method. The *P. gingivalis* suspension mentioned above was incubated with BHI containing MMC (1 mg/mL), MET-KET (1 mg/mL within 1 min), and MET-KET@MMC (1 mg/mL within 1 min) separately. 100 μL of 10-fold serial dilutions from the mixed suspension was spread onto the BHI agar plates mentioned above, and the plates were incubated for 2 d in order to count the visible numbers of CFUs. The number of CFUs was recorded, the number of CFUs was determined, and the antimicrobial efficiency was computed using the equation below

$$\text{antibacterial efficiency } (\%) = (N_C - N_E)/N_C \times 100\%$$

where N_C is the number of the control group and N_E is the number of the experimental groups.[49]

SEM. The bacteria suspension mentioned above was cultivated with sterile titanium discs in a 24-well plate for 2 d. BHI with MMC (1 mg/mL), MET-KET (1 mg/mL within 1 min), and MET-KET@MMC (1 mg/mL, within 1 min) were added into the plates and incubated for another 2 d anaerobically.[50] After the incubation, the titanium discs were placed in a 2% glutaraldehyde−cacodylate-buffered fixative solution, dehydrated in graded alcohol, and critical-point dried. The occlusal section was sputter-coated with gold palladium.[41] The SEM mentioned above was used to obtain all images of *P. gingivalis.*

Time Kill Assay. MMC (1 mg/mL), MET-KET (1 mg/mL within 1 min), and MET-KET@MMC (1 mg/mL, within 1 min) were added into BHI separately, and then, the plates were cultured anaerobically at 37 °C. Growth of *P. gingivalis* was monitored using a microplate reader every 2 h for 2 d.[51]

Live/Dead Staining of Bacteria. *P. gingivalis* suspensions mentioned above were cultivated in confocal dishes with different kinds of BHI at 1 mg/mL MMC (1 mg/mL), MET-KET, and MET-KET@MMC (1 mg/mL within 1 min), separately. After 48 h, the culture mediums were extracted, and the bacteria were stained by a Baclight Live/dead bacterial viability kit (Servicebio, China) in accordance with the instructions.[52] A confocal laser scanning microscope (Olympus FV1000, Japan) was put to use to capture the fluorescence image.[53]

Statistical Analyses. All data were presented as means ± standard deviations (SD). The IBM SPSS (IBM Corp., New York, NY, USA) was used to analyze the data set. A one-way analysis of variance and Student's *t*-test were performed to assess the significant effects of the variables. The means of each group were compared by Tukey's multiple comparison test. Statistical significance was determined by $P < 0.05$.

AUTHOR INFORMATION

Corresponding Authors

Jiyao Li − *State Key Laboratory of Oral Diseases, National Clinical Research Center for Oral Diseases, Department of Cariology and Endodontics, West China Hospital of Stomatology, Sichuan University, Chengdu 610041, China;* orcid.org/0000-0002-2701-5179; Email: jiyaoliscu@163.com

Kunneng Liang − *State Key Laboratory of Oral Diseases, National Clinical Research Center for Oral Diseases, Department of Cariology and Endodontics, West China Hospital of Stomatology, Sichuan University, Chengdu 610041, China;* orcid.org/0009-0009-3655-4228; Email: kunnengliang@scu.edu.cn

Authors

Zhaohan Yu − *State Key Laboratory of Oral Diseases, National Clinical Research Center for Oral Diseases, Department of Cariology and Endodontics, West China Hospital of Stomatology, Sichuan University, Chengdu 610041, China*

Yan Xiong − *Orthopedic Research Institute, Department of Orthopedics, West China Hospital, Sichuan University, Chengdu 610041, China*

Menglin Fan − *State Key Laboratory of Oral Diseases, National Clinical Research Center for Oral Diseases, Department of Cariology and Endodontics, West China Hospital of Stomatology, Sichuan University, Chengdu 610041, China*

Complete contact information is available at: https://pubs.acs.org/10.1021/acsomega.3c02968

Author Contributions

Z.Y. and Y.X. contributed equally to this work. J.L. and K.L. were in charge of the design and plan of the whole experiment. Z.Y. conducted the experiment. Y.X. was also in charge of the analysis of the results. M.F. provided helpful guidance in this study. Finally, Z.Y. wrote the article.

Notes

The authors declare no competing financial interest.

ACKNOWLEDGMENTS

This work was supported by the National Natural Science Foundation of China (82270970, 82170949, 81991500, and 81991501), the Key Research and Development Program of Sichuan Province (2022YFS0288 and 2023YFS0048), the Chengdu Science and Technology Support Program (2021-YF05-02061-SN), the Postdoctoral Cross Funding of Sichuan University (0040304153013), and the China Postdoctoral Foundation (2018M643507).

REFERENCES

(1) Eke, P. I.; Dye, B. A.; Wei, L.; Slade, G. D.; Thornton-Evans, G. O.; Borgnakke, W. S.; Taylor, G. W.; Page, R. C.; Beck, J. D.; Genco, R. J. Update on Prevalence of Periodontitis in Adults in the United States: NHANES 2009 to 2012. *J. Periodontol.* **2015**, *86*, 611−622.

(2) Xu, W.; Zhou, W.; Wang, H.; Liang, S. Roles of Porphyromonas gingivalis and its virulence factors in periodontitis. *Adv. Protein Chem. Struct. Biol.* **2020**, *120*, 45−84.

(3) Irshad, M.; Alam, M. K.; Alawneh, A.; Alhadi, M. A.; Alhadi, A. A.; Almunajem, Y. S.; Alanezi, F. F.; Al Sagoor, S. A.; Bajawi, A. M.; Alfawzan, A. A.; et al. Characterization and Antimicrobial Suscept-

https://doi.org/10.1021/acsomega.3c02968
ACS Omega 2023, 8, 25441−25452

ibility of Pathogens Associated with Periodontal Abscess. *Antibiotics* **2020**, *9*, 654.
(4) Kim, S. J.; Seo, J. T. Selection of analgesics for the management of acute and postoperative dental pain: a mini-review. *J. Periodontal Implant Sci.* **2020**, *50*, 68−73.
(5) Ashley, P. F.; Parekh, S.; Moles, D. R.; Anand, P.; MacDonald, L. C. Preoperative analgesics for additional pain relief in children and adolescents having dental treatment. *Cochrane Database Syst. Rev.* **2016**, *2016*, Cd008392.
(6) Alobaid, M. A.; Alobaid, S.; Alshahrani, M. Comparison of the Views of the General Dental Practitioners and Dental Interns in Asir, Saudi Arabia on Antibiotic Prescription for Endodontic Therapy: A Cross-Sectional Study. *Infect. Drug Resist.* **2021**, *14*, 3001−3009.
(7) Carlsen, D. B.; Durkin, M. J.; Gibson, G.; Jurasic, M. M.; Patel, U.; Poggensee, L.; Fitzpatrick, M. A.; Echevarria, K.; McGregor, J.; Evans, C. T.; et al. Concordance of antibiotic prescribing with the American Dental Association acute oral infection guidelines within Veterans' Affairs (VA) dentistry. *Infect. Control Hosp. Epidemiol.* **2021**, *42*, 1422−1430.
(8) Fan, X.; Yang, F.; Nie, C.; Ma, L.; Cheng, C.; Haag, R. Biocatalytic Nanomaterials: A New Pathway for Bacterial Disinfection. *Adv. Mater.* **2021**, *33*, No. e2100637.
(9) Madhumathi, K.; Rubaiya, Y.; Doble, M.; Venkateswari, R.; Sampath Kumar, T. S. Antibacterial, anti-inflammatory, and bone-regenerative dual-drug-loaded calcium phosphate nanocarriers-in vitro and in vivo studies. *Drug Delivery Transl. Res.* **2018**, *8*, 1066−1077.
(10) Atzeni, F.; Masala, I. F.; Bagnasco, M.; Lanata, L.; Mantelli, F.; Sarzi-Puttini, P. Comparison of Efficacy of Ketoprofen and Ibuprofen in Treating Pain in Patients with Rheumatoid Arthritis: A Systematic Review and Meta-Analysis. *Pain Ther.* **2021**, *10*, 577−588.
(11) Ghosh, S. Metabolomic Studies for Metabolic Alterations Induced by Non-Steroidal Anti-Inflammatory Drugs: Mini Review. *Biomolecules* **2021**, *11*, 1456.
(12) Ré, A. C.; Ferreira, M. P.; Freitas, O.; Aires, C. P. Local antibiotic delivery in periodontitis: drug release and its effect on supragingival biofilms. *Biofouling* **2016**, *32*, 1061−1066.
(13) Munar-Bestard, M.; Llopis-Grimalt, M. A.; Ramis, J. M.; Monjo, M. Comparative In Vitro Evaluation of Commercial Periodontal Gels on Antibacterial, Biocompatibility and Wound Healing Ability. *Pharmaceutics* **2021**, *13*, 1502.
(14) (a) Elder, D. P.; Holm, R.; Diego, H. L. Use of pharmaceutical salts and cocrystals to address the issue of poor solubility. *Int J Pharm* **2013**, *453*, 88−100. From NLM (b) Wang, B.; Liu, F.; Xiang, J.; He, Y.; Zhang, Z.; Cheng, Z.; Liu, W.; Tan, S. A critical review of spray-dried amorphous pharmaceuticals: Synthesis, analysis and application. *Int. J. Pharm.* **2021**, *594*, 120165.
(15) Tang, R.; Li, R.; Li, H.; Ma, X. L.; Du, P.; Yu, X. Y.; Ren, L.; Wang, L. L.; Zheng, W. S. Design of Hepatic Targeted Drug Delivery Systems for Natural Products: Insights into Nomenclature Revision of Nonalcoholic Fatty Liver Disease. *ACS Nano* **2021**, *15*, 17016−17046.
(16) Di Cristo, F.; Valentino, A.; De Luca, I.; Peluso, G.; Bonadies, I.; Calarco, A.; Di Salle, A. PLA Nanofibers for Microenvironmental-Responsive Quercetin Release in Local Periodontal Treatment. *Molecules* **2022**, *27*, 2205.
(17) Brouwers, J.; Brewster, M. E.; Augustijns, P. J. J. o. p. s. Supersaturating drug delivery systems: the answer to solubility-limited oral bioavailability? *J. Pharm. Sci.* **2009**, *98*, 2549−2572.
(18) He, X. *Developing solid oral dosage forms*; Elsevier, 2009, pp 407−441.Integration of physical, chemical, mechanical, and bio-pharmaceutical properties in solid oral dosage form development
(19) Yao, Y.; Dai, X.; Tan, Y.; Chen, Y.; Liao, C.; Yang, T.; Chen, Y.; Yu, Y.; Zhang, S. Deep Drug Penetration of Nanodrug Aggregates at Tumor Tissues by Fast Extracellular Drug Release. *Adv. Healthcare Mater.* **2021**, *10*, No. e2001430.
(20) Zardan Gomez de la Torre, T.; Lindmark, T.; Cheung, O.; Bergstrom, C.; Stromme, M. Bioavailability of Celecoxib Formulated with Mesoporous Magnesium Carbonate-An In Vivo Evaluation. *Molecules* **2022**, *27*, 6188.
(21) Głowniak, S.; Szczęśniak, B.; Choma, J.; Jaroniec, M. Advances in Microwave Synthesis of Nanoporous Materials. *Adv. Mater.* **2021**, *33*, No. e2103477.
(22) Bai, Y. M.; Mao, J.; Li, D. X.; Luo, X. J.; Chen, J.; Tay, F. R.; Niu, L. N. Bimodal antibacterial system based on quaternary ammonium silane-coupled core-shell hollow mesoporous silica. *Acta Biomater.* **2019**, *85*, 229−240.
(23) Zhang, P.; Forsgren, J.; Strømme, M. Stabilisation of amorphous ibuprofen in Upsalite, a mesoporous magnesium carbonate, as an approach to increasing the aqueous solubility of poorly soluble drugs. *Int. J. Pharm.* **2014**, *472*, 185−191.
(24) Zhang, P.; Zardán Gómez de la Torre, T.; Welch, K.; Bergström, C.; Strømme, M. Supersaturation of poorly soluble drugs induced by mesoporous magnesium carbonate. *Eur. J. Pharm. Sci.* **2016**, *93*, 468−474.
(25) Yang, J.; Alvebratt, C.; Zhang, P.; Zardán Gómez de la Torre, T.; Strømme, M.; Bergström, C. A. S.; Welch, K. Enhanced release of poorly water-soluble drugs from synergy between mesoporous magnesium carbonate and polymers. *Int. J. Pharm.* **2017**, *525*, 183−190.
(26) Yang, J.; Alvebratt, C.; Lu, X.; Bergstrom, C. A. S.; Stromme, M.; Welch, K. Amorphous magnesium carbonate nanoparticles with strong stabilizing capability for amorphous ibuprofen. *Int. J. Pharm.* **2018**, *548*, 515−521.
(27) Stubelius, A.; Sheng, W.; Lee, S.; Olejniczak, J.; Guma, M.; Almutairi, A. Disease-Triggered Drug Release Effectively Prevents Acute Inflammatory Flare-Ups, Achieving Reduced Dosing. *Small* **2018**, *14*, No. e1800703.
(28) Katsiotis, C. S.; Åhlén, M.; Strømme, M.; Welch, K. 3D-Printed Mesoporous Carrier System for Delivery of Poorly Soluble Drugs. *Pharmaceutics* **2021**, *13*, 1096.
(29) Li-Hong, W.; Xin, C.; Hui, X.; Li-Li, Z.; Jing, H.; Mei-Juan, Z.; Jie, L.; Yi, L.; Jin-Wen, L.; Wei, Z.; et al. A novel strategy to design sustained-release poorly water-soluble drug mesoporous silica microparticles based on supercritical fluid technique. *Int. J. Pharm.* **2013**, *454*, 135−142.
(30) Konno, T.; Kinuno, K. Physical and chemical changes of medicinals in mixtures with adsorbents in the solid state. II. Application of reduced pressure treatment for the improvement of dissolution of flufenamic acid. *Chem. Pharm. Bull.* **1989**, *37*, 2481−2484.
(31) Ge, Y.; Wang, K.; Li, H.; Tian, Y.; Wu, Y.; Lin, Z.; Lin, Y.; Wang, Y.; Zhang, J.; Tang, B. An Mg-MOFs based multifunctional medicine for the treatment of osteoporotic pain. *Mater. Sci. Eng., C* **2021**, *129*, 112386.
(32) Yu, J.; Yang, H.; Li, K.; Lei, J.; Zhou, L.; Huang, C. A novel application of nanohydroxyapatite/mesoporous silica biocomposite on treating dentin hypersensitivity: An in vitro study. *J. Dent.* **2016**, *50*, 21−29.
(33) Marano, S.; Barker, S. A.; Raimi-Abraham, B. T.; Missaghi, S.; Rajabi-Siahboomi, A.; Craig, D. Q. M. Development of micro-fibrous solid dispersions of poorly water-soluble drugs in sucrose using temperature-controlled centrifugal spinning. *Eur. J. Pharm. Biopharm.* **2016**, *103*, 84−94.
(34) Chiani, E.; Beaucamp, A.; Hamzeh, Y.; Azadfallah, M.; Thanusha, A. V.; Collins, M. N. Synthesis and characterization of gelatin/lignin hydrogels as quick release drug carriers for Ribavirin. *Int. J. Biol. Macromol.* **2023**, *224*, 1196−1205.
(35) Wang, D.; Xu, X.; Zhang, K.; Sun, B.; Wang, L.; Meng, L.; Liu, Q.; Zheng, C.; Yang, B.; Sun, H. Codelivery of doxorubicin and MDR1-siRNA by mesoporous silica nanoparticles-polymerpolyethylenimine to improve oral squamous carcinoma treatment. *Int. J. Nanomed.* **2017**, *13*, 187−198.
(36) Usui, M.; Onizuka, S.; Sato, T.; Kokabu, S.; Ariyoshi, W.; Nakashima, K. Mechanism of alveolar bone destruction in periodontitis - Periodontal bacteria and inflammation. *Jpn. Dent. Sci. Rev.* **2021**, *57*, 201−208.
(37) Bozkurt, S. B.; Hakki, S. S.; Hakki, E. E.; Durak, Y.; Kantarci, A. Porphyromonas gingivalis Lipopolysaccharide Induces a Pro-inflam-

https://doi.org/10.1021/acsomega.3c02968
ACS Omega 2023, 8, 25441−25452

matory Human Gingival Fibroblast Phenotype. *Inflammation* **2017**, *40*, 144−153.
(38) Gao, H.; Zhang, X.; Zheng, Y.; Peng, L.; Hou, J.; Meng, H. S100A9-induced release of interleukin (IL)-6 and IL-8 through toll-like receptor 4 (TLR4) in human periodontal ligament cells. *Mol. Immunol.* **2015**, *67*, 223−232.
(39) Seong, J.; Lee, J.; Lim, Y. K.; Yoon, W. J.; Jung, S.; Kook, J. K.; Lee, T. H. Osmunda japonica Extract Suppresses Pro-Inflammatory Cytokines by Downregulating NF-κB Activation in Periodontal Ligament Fibroblasts Infected with Oral Pathogenic Bacteria. *Int. J. Mol. Sci.* **2020**, *21*, 2453.
(40) Welch, K.; Latifzada, M. A.; Frykstrand, S.; Strømme, M. Investigation of the Antibacterial Effect of Mesoporous Magnesium Carbonate. *ACS Omega* **2016**, *1*, 907−914.
(41) Yu, Z.; Tao, S.; Xu, H. H. K.; Weir, M. D.; Fan, M.; Liu, Y.; Zhou, X.; Liang, K.; Li, J. Rechargeable adhesive with calcium phosphate nanoparticles inhibited long-term dentin demineralization in a biofilm-challenged environment. *J. Dent.* **2021**, *104*, 103529.
(42) Reda, R. I.; Wen, M. M.; El-Kamel, A. H. Ketoprofen-loaded Eudragit electrospun nanofibers for the treatment of oral mucositis. *Int. J. Nanomed.* **2017**, *12*, 2335−2351.
(43) Liang, K.; Xiao, S.; Liu, H.; Shi, W.; Li, J.; Gao, Y.; He, L.; Zhou, X.; Li, J. 8DSS peptide induced effective dentinal tubule occlusion in vitro. *Dent. Mater.* **2018**, *34*, 629−640.
(44) Zhang, X.; Xing, H.; Zhao, Y.; Ma, Z. Pharmaceutical Dispersion Techniques for Dissolution and Bioavailability Enhancement of Poorly Water-Soluble Drugs. *Pharmaceutics* **2018**, *10*, 74.
(45) Cheng, R.; Feng, Y.; Zhang, R.; Liu, W.; Lei, L.; Hu, T. The extent of pyroptosis varies in different stages of apical periodontitis. *Biochim. Biophys. Acta, Mol. Basis Dis.* **2018**, *1864*, 226−237.
(46) Gölz, L.; Memmert, S.; Rath-Deschner, B.; Jäger, A.; Appel, T.; Baumgarten, G.; Götz, W.; Frede, S. Hypoxia and P. gingivalis synergistically induce HIF-1 and NF-κB activation in PDL cells and periodontal diseases. *Mediators Inflammation* **2015**, *2015*, 1−12.
(47) Zhang, C.; Kuang, X.; Zhou, Y.; Peng, X.; Guo, Q.; Yang, T.; Zhou, X.; Luo, Y.; Xu, X. A Novel Small Molecule, ZY354, Inhibits Dental Caries-Associated Oral Biofilms. *Antimicrob. Agents Chemother.* **2019**, *63*, No. e02414.
(48) Livak, K. J.; Schmittgen, T. D. J. m. Analysis of relative gene expression data using real-time quantitative PCR and the 2− ΔΔCT method. *Methods* **2001**, *25*, 402−408.
(49) Deng, Y.; Shi, J.; Chan, Y. K.; Bai, D.; Shu, R.; Shi, X.; Li, Y.; Li, L.; Yang, X.; Yang, W. Heterostructured Metal-Organic Frameworks/Polydopamine Coating Endows Polyetheretherketone Implants with Multimodal Osteogenicity and Photoswitchable Disinfection. *Adv. Healthcare Mater.* **2022**, *11*, No. e2200641.
(50) Zheng, Y.; Li, J.; Liu, X.; Sun, J. Antimicrobial and osteogenic effect of Ag-implanted titanium with a nanostructured surface. *Int. J. Nanomed.* **2012**, *7*, 875−884.
(51) Kim, K.; Kim, D.; Lee, H.; Lee, T. H.; Kim, K. Y.; Kim, H. New Pyrimidinone-Fused 1,4-Naphthoquinone Derivatives Inhibit the Growth of Drug Resistant Oral Bacteria. *Biomedicines* **2020**, *8*, 160.
(52) Tao, S.; Yang, X.; Liao, L.; Yang, J.; Liang, K.; Zeng, S.; Zhou, J.; Zhang, M.; Li, J. A novel anticaries agent, honokiol-loaded poly(amido amine) dendrimer, for simultaneous long-term antibacterial treatment and remineralization of demineralized enamel. *Dent. Mater.* **2021**, *37*, 1337−1349.
(53) Tao, S.; Su, Z.; Xiang, Z.; Xu, H. H. K.; Weir, M. D.; Fan, M.; Yu, Z.; Zhou, X.; Liang, K.; Li, J. Nano-calcium phosphate and dimethylaminohexadecyl methacrylate adhesive for dentin remineralization in a biofilm-challenged environment. *Dent. Mater.* **2020**, *36*, e316−e328.

https://doi.org/10.1021/acsomega.3c02968
ACS Omega 2023, 8, 25441−25452